Proceedings of ASME Turbo Expo 2011
GT2011
June 6-10, 2011, Vancouver, British Columbia, Canada

GT2011-45117

APPLICATION OF A CFD-BASED FILM COOLING MODEL TO A GAS TURBINE VANE CASCADE WITH CYLINDRICAL AND SHAPED HOLE ENDWALL FILM COOLING

Tilman auf dem Kampe
Stefan Völker
Fossil Power Generation Division
Siemens AG, Energy Sector
45473 Mülheim a. d. Ruhr, Germany
Email: tilman.aufdemkampe@siemens.com

ABSTRACT

This paper presents the application of a CFD-based film cooling model to a gas turbine vane cascade test rig. The experimental investigations feature aerodynamic and endwall film cooling measurements on a first stage gas turbine vane in a linear cascade. An extended version of a previously developed cylindrical hole film cooling model has been employed, which now includes modeling of shaped hole cooling flows.

The computational domain extends approximately one axial chord length upstream of the leading edge and downstream of the trailing edge of the vane. Adjacent solid parts are included by means of a conjugate heat transfer analysis to account for conduction effects. A hybrid mesh with resolved boundary layers and high spatial mesh resolution in the near-wall region is being used. This meshing approach ensures that the near-wall mesh resolution requirements of the film cooling model are satisfied, while maintaining a manageable total node count.

Results obtained using the film cooling model are compared to surface distributions of film cooling effectiveness from the experimental cascade. Due to the moderate node count ($\approx 3.5 \times 10^6$)*, CFD calculations including film cooling flows can be performed at comparatively low computational cost. The film cooling model, which previously had been validated against flat plate measurement data and applied to single cooling hole configurations only, is therefore shown to be a viable tool for the thermal design of gas turbine components with film cooling.*

NOMENCLATURE

Latin Symbols

A-E	Coolant supply cavities
D	Hole diameter
H	Vane height
L	Length
P	Pitch
P, S	Shaped hole rows
t	Calculation time
T	Temperature
X,Y,Z	Cartesian coordinates

Greek Symbols

η	Film cooling effectiveness
λ_s	Stagger angle
λ	Thermal conductivity

Subscripts

ax	Axial
bsl	Baseline
c	Chord
m	Main flow
pl	Plenum
rec	Recovery
ref	Reference value
w	Wall

Abbreviations

CFD	Computational fluid dynamics
SST	Shear stress transport

INTRODUCTION

Film cooling is one of the most important cooling technologies for gas turbine vanes and blades. Although it has been used for decades, its potential to help increase turbine inlet temperatures and thus engine efficiency and output is still significant. Since film cooling is unfavorable from a thermodynamic cycle point of view, a highly efficient use of film cooling is called for. Due to its great potential, many studies have been undertaken to improve the understanding of film cooling flows and the way they interact with the hot gas flow, in an attempt to find means to leverage the greatest possible benefit from film cooling.

Current methods for the thermal design of film-cooled components are usually based on correlations of laterally averaged film cooling effectiveness that have been obtained from experimental results, for example by L'Ecuyer and Soechting [1] or Baldauf [2]. 3D-CFD calculations of the film cooled component are usually performed neglecting film cooling flows entirely. The effect of film cooling is accounted for in a post-processing step, which involves applying the aforementioned film cooling effectiveness correlations. The advantage of this approach is that it is very fast and predictions of film cooling effectiveness can be obtained rather quickly, which is favorable from a designer's point of view. On the other hand, the applicability of correlations obtained under experimental conditions to gas turbine relevant cases is limited. This is particularly true for endwall film cooling, as the flow in this region is more heavily influenced by secondary flows than on airfoil pressure and suction side, cp. e.g. Colban and Thole [3] and Colban et al. [4].

A more general approach accounting for film cooling flows within a CFD environment allows to include more of the physically relevant effects. Fully resolving the small scale geometry and flow features of film cooling holes relative to the large scale component is possible as has been shown by Goormans-Francke et al. [5], but computational requirements are still very high. Even with today's computational resources, running high resolution CFD models is impractical for day-to-day use. Furthermore, significant modeling effort is required to build the CFD models and different film cooling configurations cannot be investigated and compared easily.

To mitigate the extreme computational and modeling requirements of high resolution CFD calculations, attempts have been made to efficiently model the film cooling flows in a CFD environment. First approaches in two-dimensional space have been presented by Miller and Crawford [6]. More recently, models have also been developed for application in 3D-CFD environments. Among the first were the approaches presented by Heidmann and Hunter [7] and Dahlander [8] using simple volumetric source terms. More recently, Burdet et al. [9] presented a model that inserts the coolant flow through an injection plane within the fluid domain located just downstream of the coolant hole exit and uses an immersed boundary condition method to model the shape of the jet upstream of the injection plane and its blockage effect. Tartinville and Hirsch [10] presented another injection-based approach that uses face cell source terms at wall-adjacent cells.

In this paper, an extended version of the film cooling model by auf dem Kampe and Völker [11] is employed. It uses distributed volumetric source terms to introduce the coolant into the computational domain and model the blockage effect at the same time. Source terms are calculated individually for each computational node within a defined source volume in the vicinity of a cooling hole and for each transport equation. Size and shape of the source volume and the local source terms are calculated based on a correlation of the local flow field. The correlation accounts among others for the effects of blowing and density ratio, inclination and compound angle of the hole, see auf dem Kampe et al. [12]. Distributed source terms are calculated for velocity components and temperature, mimicking the aerodynamic and thermal flow field at the cooling hole exit. A local integral flux conservation method ensures that the correct amount of mass, momentum and energy is added for each hole. The current version of the film cooling model uses constant average values as source terms for the turbulence transport quantities, i.e. it does not leverage the potential of using distributed sources for these quantities.

Previously, this film cooling model has successfully been applied to flat plate configurations and single hole ejection through cylindrical holes only [11]. Validation has shown that flow features like jet lift-off can be resolved provided that a sufficiently fine mesh with a minimum resolution of three nodes per hole diameter is employed. Laterally averaged film cooling effectiveness could be predicted to within ± 0.05. For this study, the flow field correlations have been extended to also model laidback fan shaped diffuser holes. The model extension has been developed based on a detailed CFD validation for shaped hole film cooling by auf dem Kampe et al. [13] using a film cooling test rig at the Institute of Thermal Turbomachinery in Karlsruhe, see Heneka et al. [14]. New parameters that have been taken into consideration for diffuser holes include diffuser area ratio and cylindrical starting length aside from the parameters that influence both diffuser and cylindrical holes, for example blowing and density ratio. Further details of the model extension for laidback fan shaped diffuser holes may not be given here for proprietary reasons.

The intent of this study is to show the applicability of the auf dem Kampe and Völker [11] film cooling model approach to a gas turbine relevant test case. It is employed to model rows of laidback fan shaped holes on a flat endwall of a linear vane cascade and is shown to agree reasonably well with experimental data by Kunze et al. [15]. It is further shown that the film cooling model can be executed to model an arbitrary number of film cooling holes with negligible additional modeling effort and computational overhead for an example case featuring a total of 253 cooling holes.

EXPERIMENTAL SETUP

The experimental investigations considered in this study have been performed in the Low Speed Research Cascade Wind Tunnel at the Technical University of Dresden. The investigated geometry features a linear cascade with 6 filleted prismatic airfoil profiles. A flat endwall with film cooling holes is located in the center of the cascade, where a quasi-periodic flow field may be assumed. Airfoils were manufactured with a wooden core and a smooth rubber coating, while low-conductivity perspex ($\lambda = 0.19$ W/mK) was used for the film-cooled endwall. Basic geometrical features of the investigated vane are provided in Table 1.

TABLE 1. Profile data

Pitch	P	184 mm
Chord length	L_c	188.4 mm
Vane height	H	300 mm
Axial chord length	L_{ax}	102.7 mm
Stagger angle	λ_s	34.8°

The wind tunnel supplies a continuous approach flow at approximately 22m/s and at temperatures slightly higher than ambient temperature, resulting in an inlet Reynolds number of $2.6 \cdot 10^5$ and an exit Reynolds number of $8.1 \cdot 10^5$ based on the chord length. The displacement boundary layer thickness at the inlet was 4.655mm with a shape factor of 1.179. Heated carbon dioxide was used to simulate the coolant, i.e. temperature gradients in this experimental facility are opposite to gradients under engine conditions. The use of carbon dioxide allowed that density ratios greater than unity could be achieved. The total temperature difference between coolant and main flow was on the order of 20K. A temperature sensitive paint method was used to measure surface temperatures on the flat endwall. A detailed description of the test rig and the measurement technique has been documented by Kunze et al. [16].

The flat endwall features a total of 253 film cooling holes, 47 of which are cylindrical while 206 are laidback fan shaped diffuser holes. The coolant is supplied through 5 different supply chambers (A-E) in which the flow is quiescent. The diffuser

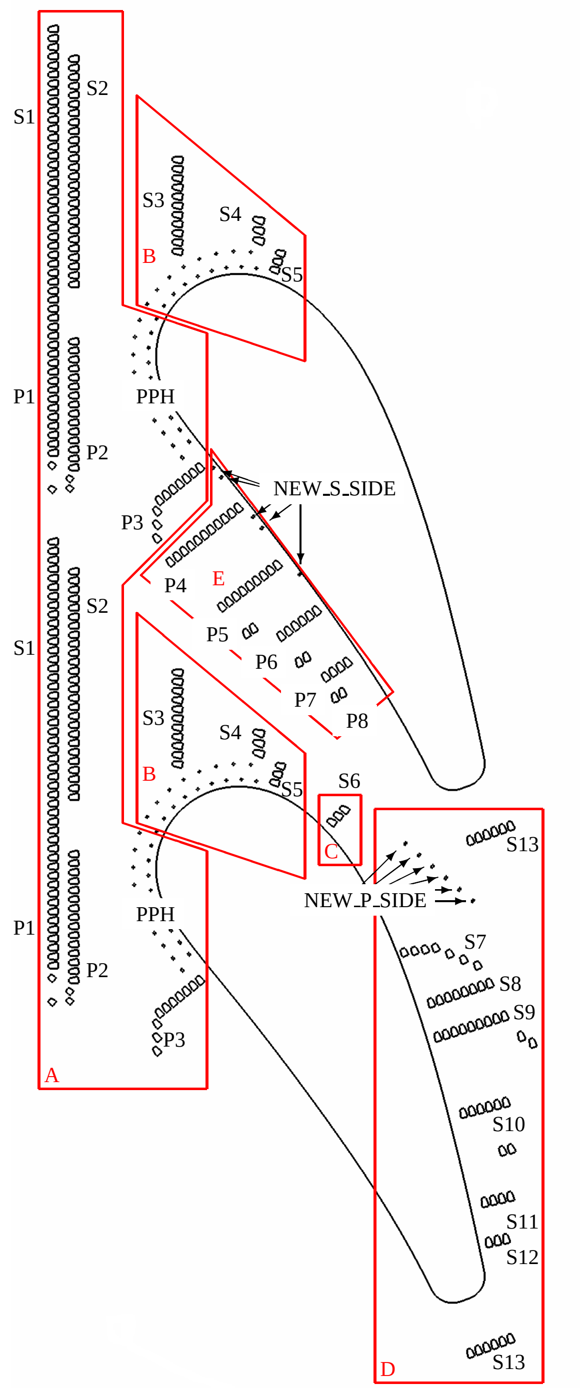

FIGURE 1. Schematic of endwall test plate with cooling hole row and supply cavity nomenclature

holes are arranged in 21 rows of holes (P1-P8, S1-S13) along the suction side and pressure side of the airfoil, while the cylindrical cooling holes are used almost exclusively around the leading

TABLE 2. Coolant supply scheme

Cavity	Rows supplied	Holes per passage	Blowing ratio	Density ratio
A	S1-S2, P1-P3, PPH (partially)	123	1 ... 2.5	1.38
B	S3-S5, PPH (partially)	33	1.4 ... 2.9	
C	S6	3	1.6 ... 1.8	
D	S7-S13, NEW_P_SIDE	53	0.5 ... 1.0	
E	P4-P8, NEW_S_SIDE	41	1.8 ... 3.0	
Total		253	0.5 ... 3.0	1.38

edge of the profile. The nomenclature for supply chambers and cooling hole rows can be derived from Figure 1. Table 2 gives the coolant supply scheme, i.e. which cavity supplies which coolant row and the ranges of blowing an density ratios.

Measurements of film cooling effectiveness were obtained for each cooling hole row separately at three different approach flow incidence angles. For the purpose of this study, the measurements with design point approach flow were used. The entire measurement campaign has been documented in detail by Kunze et al. [15].

Due to the small temperature difference between coolant and main flow, the experimenters found that the measurement results were influenced noticeably by heat conduction effects, for which they later introduced a correction. This conduction correction only considers the heat exchange between fluid and solid as well as the conduction effects in the endwall due to the coolant flowing through the holes. Therefore, heat conduction effects from cavity walls to the hot side of the endwall have not been included. Furthermore, lateral heat conduction between coolant streaks and less cooled neighboring regions still affects the measurement results. This means that a dataset with truly adiabatic film cooling effectiveness could not be obtained. When attempting a quantitative comparison with the CFD predictions, this has to be kept in mind.

CFD SETUP

The computational domain is depicted in Figure 2 and includes both a fluid and a solid domain. The fluid domain extends from approximately one axial chord length ($0.86l_{ax}$) upstream of the leading edge to one axial chord length ($0.98l_{ax}$) downstream of the trailing edge of the airfoil. In the spanwise direction, the domain extends from the film cooled flat endwall up to midspan. In the pitchwise direction, the domain extends one pitch, enveloping the profile. The location of the pitchwise boundaries has been chosen carefully as to avoid interference with film cooling holes on the endwall. The fillet radii of the profile at its junction with the endwall have been included in the CFD model. The solid domain is a simple flat plate with a constant thickness of aprximately $8D$ that is attached to the film cooled endwall. It has been included to allow for lateral heat conduction in the solid, which is a physical effect that has been found to have a noticeable influence on the experimental results. Therefore, to allow for a comparison with the experimental results, the flat plate had to be included in the CFD model.

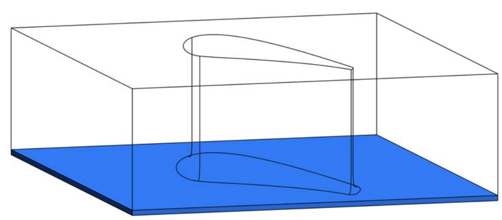

FIGURE 2. Sketch of fluid (wire frame) and solid (solid coloured) computational domain

A hybrid mesh, resolving boundary layers on endwall and airfoil has been used. This was done by placing a hexahedral O-grid around the airfoil, whereas prism layers were used on the endwall. Outside of boundary layers, a tetrahedral mesh was used. ANSYS ICEM was used for mesh generation. One advantage of the film cooling model is that its mesh resolution requirements are significantly lower than for a fully resolved film cooling simulation. The turning and squeezing of the film jet in the immediate vicinity of the hole exit is what requires a highly resolved mesh. These effects are included in the film cooling model and imposed locally onto the CFD, thereby reducing mesh requirements by about an order of magnitude. The minimum mesh resolution requirement when using the film cooling model has been reported as 3 nodes per hole diameter [11]. This requirement was satisfied on the entire endwall as can be seen in Figure 3 which shows a detailed view of the platform mesh near rows P3 and P4 with the cooling hole breakouts indicated.

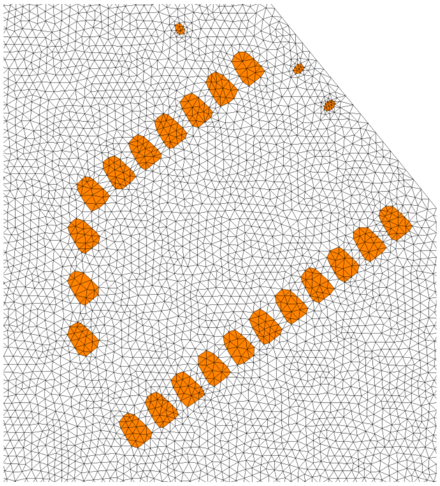

FIGURE 3. Platform mesh near rows P3 and P4

Adiabatic, no slip wall boundary conditions were imposed on the airfoil surface, while a conjugate heat transfer interface was specified at the endwall. A symmetry boundary condition was imposed at midspan to reduce the size of the computational domain. A full-span CFD calculation was performed to verify the validity of the half-span symmetry assumption. Translational periodicity was assumed at the pitchwise boundaries. Measured spanwise velocity and turbulence intensity profiles of the approach flow boundary layer were used as inlet boundary condition along with a fixed approach flow angle.

The outlet is treated as a constant static pressure outlet. All solid boundaries, except for where the solid domain is attached to the fluid domain, are adiabatic walls. Therefore, the solid domain only provides a means to allow for lateral heat conduction, no energy leaves the computational domain.

ANSYS CFX was used as a flow solver. The k-ω-SST turbulence model by Menter [17] with Reattachment Modification was used to model the turbulence transport. The film cooling model by auf dem Kampe and Völker [11] with an extension for laidback fan shaped diffuser holes was employed to model the film cooling flows.

To set up the film cooling model hole specific mass flow and coolant supply temperature were used according to the experiments. In addition, geometric hole parameters such as hole inlet and outlet location, hole diameter, diffuser area ratio and cylindrical starting length were required. The full set of input parameters for the film cooling model was then calculated using a CFD solution of the flow field without film cooling, which also served as initial solution for all film cooling calculations. Further film cooling model input parameters include blowing ratio, density ratio and approach flow direction and therefore require free stream information.

Note that correct hole specific mass flow rates and coolant discharge temperatures are crucial for proper performance of the film cooling model. Unfortunately, both mass flow and coolant supply temperature could only be obtained with some degree of uncertainty. In the experiments, the coolant mass flow was measured at the inlet to the coolant cavity. Therefore, the total mass flow through all opened film cooling holes was well known, but the mass flow for each single hole was not. The experimenters suggested to distribute the coolant flow based on the flowpath-side static wall pressure. Hole specific mass flow rates based on this assumption have been used as boundary condition for the film cooling model. Coolant supply temperatures were also not measured directly in the experiments. The total temperature of the coolant in the quiescent cavity was measured. Yet the discharge temperature of the coolant at hole exit is different due to heat exchange between coolant and solid upstream of the cooling hole exit. The experimenters calculated the discharge temperature based on correlation based estimates of the heat flux from fluid to solid and these values were used to set up the film cooling model. If the total temperature difference between coolant and freestream is only 20K as in this case, an uncertainty of $\pm$1K in discharge temperature results in a noticeable uncertainty of $\pm$0.05 in film cooling effectiveness. These uncertainties have to be kept in mind when attempting a quantitative comparison between CFD based predictions and experimental data.

RESULTS

Results are presented in terms of contour plots of film cooling effectiveness for both experimental and computational results. Film cooling effectiveness is calculated according to Equation 1, which is in accordance with the experimenter's definition, cp. Kunze et al. [15]. $T_{rec,m}$ denotes the recovery temperature of the free stream flow, T_w the wall temperature and T_{pl} the coolant temperature in the plenum cavity. The recovery temperature for this low speed wind tunnel is assumed to be equal to the mainflow static temperature.

$$\eta = \frac{T_w - T_{rec,m}}{T_{pl} - T_{rec,m}} \qquad (1)$$

Results are grouped based on the feeding cavities (D, B and E, A), which also correspond to the cooling hole locations in the passage. Note that each coolant row was tested separately except for rows S4 and S5 which were measured jointly, as well as rows S12 and S13. Therefore, all measurement results are not influenced by upstream film cooling ejection, investigating superposition effects was not the scope of the experiments. No measurements were obtained for rows P7, P8, S6, S8 and the cylindrical hole groups PPH, NEW_P_SIDE and NEW_S_SIDE.

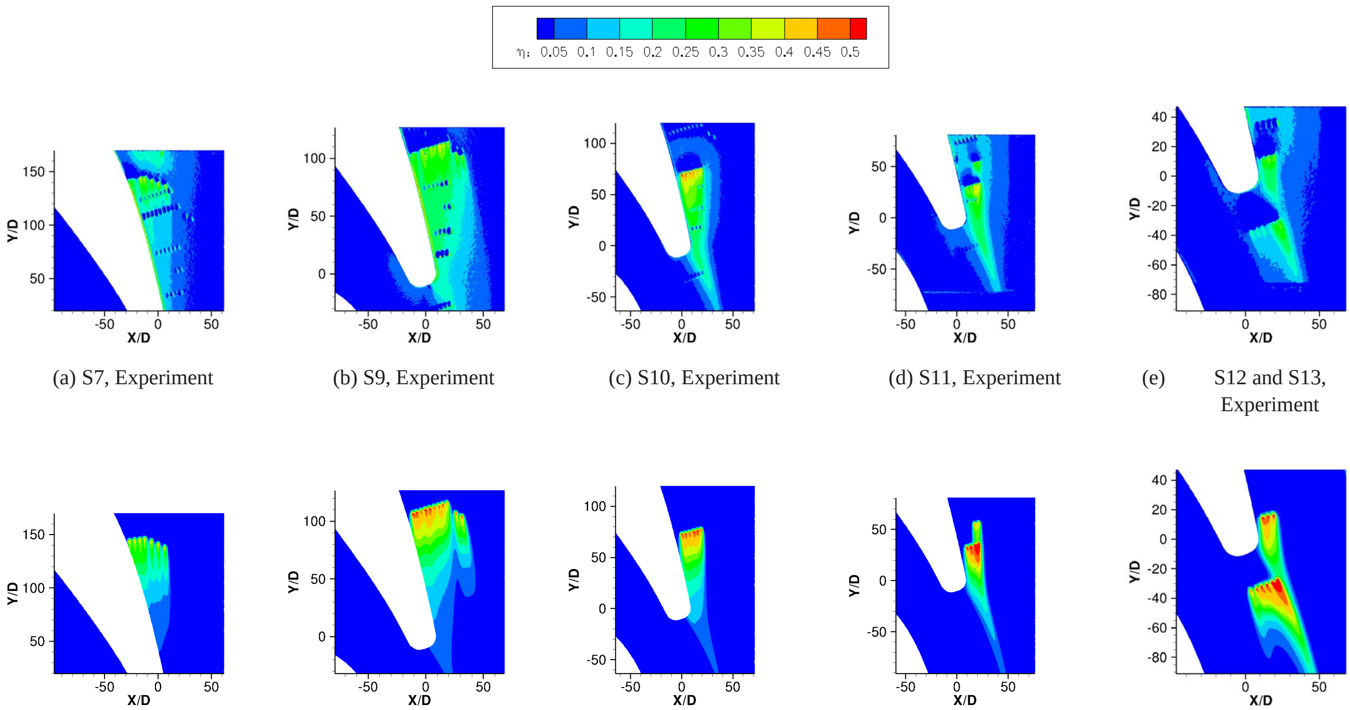

(a) S7, Experiment (b) S9, Experiment (c) S10, Experiment (d) S11, Experiment (e) S12 and S13, Experiment

(f) S7, CFD (g) S9, CFD (h) S10, CFD (i) S11, CFD (j) S12 and S13, CFD

FIGURE 4. Cavity D cooling hole rows S7, S9-S13

Cavity D - Cooling rows downstream of the passage

Figure 4 summarizes the results in terms of contour plots of film cooling effectiveness for rows S7 and S9 through S13, which are all fed with coolant by cavity D. All of these coolant rows are located in the aft section of the vane passage, which is only weakly affected by secondary flows. Higher row numbers indicate further downstream row location, row S13 is farthest downstream in the wake region of the trailing edge, see Figure 1. The top row of Figure 4 shows experimental data, the bottom row shows the corresponding computational results.

The agreement between CFD and experiment in this region of the vane passage is very good in terms of coolant coverage. In terms of the level of cooling effectiveness, the agreement is very good for row S7, see Figures 4(a) and 4(f). For coolant rows S9 through S13, the level of cooling effectiveness near the hole is overpredicted by up to 100% locally, while it is slightly underpredicted by about 10% on average further downstream. Deviations are most noticeable for coolant rows S11 through S13.

The overprediction of film cooling effectiveness near the hole may be attributable to the use of constant, film cooling parameter independent source terms for turbulence quantities, which appear to underestimate the turbulent mixing of the jet.

The underprediction of cooling effectiveness further downstream of cooling holes can be attributed to the following effect, which is obvious in the experimental results presented here. There is a slightly increased level of film cooling effectiveness in regions not covered by coolant. This is most apparent in Figures 4(d) and 4(e), which show significant film cooling effectiveness upstream of and next to the cooling rows, although the experimental data was corrected in order to remove the effect of heat exchange between coolant and solid in the hole. The presence of regions of non-zero cooling effectiveness where no coolant is present reveals that there is additional conduction taking place between coolant cavity and main flowpath. This is further corroborated by the fact that the extent of the regions showing elevated cooling effectiveness aligns well with the geometry of the underlying cavity.

Neglecting this influence has two main effects. First of all, using a discharge temperature that neglects this heat exchange leads to an overprediction of cooling effectiveness near the hole exit. Secondly, the heat conduction from plenum to main flowpath through the endwall leads to an almost uniform elevated cooling effectiveness on the platform above the coolant cavity, causing higher levels of cooling effectiveness in regions far downstream of the coolant ejection. As the aforementioned effects are not accounted for in the calculation of coolant discharge temperatures, and as the underlying cavities are not part of the CFD model, they cannot be captured in the CFD and thus help

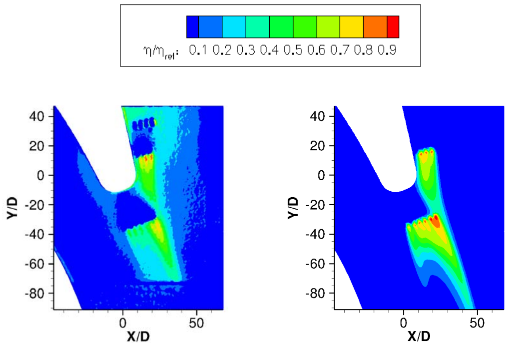

(a) S12 and S13, Experiment

(b) S12 and S13, CFD

FIGURE 5. Normalized cooling effectiveness for rows S12 and S13

explain the observed deviations.

However, it is important to note that the footprint of the coolant including the decay of cooling effectiveness is still represented quite well. Figure 5 shows a comparison of the results for rows S12 and S13 (for which the level mismatch was most significant), with the cooling effectiveness normalized to range from zero to unity in both plots. This representation allows to consider the downstream effectiveness decay, removing the effect of discharge temperature uncertainty. It can be seen that the qualitative behavior is captured very well by the film cooling model. Using an appropriate discharge temperature therefore promises to deliver reasonable results both qualitatively and quantitatively.

Cavities B and E - Cooling rows in the passage

Results for cooling rows fed through cavities B and E are presented in Figure 6 in the same fashion as previously for cavity D (Experiments in top row, corresponding computational results below). These cooling rows are located in the mid-section of the vane passage, see Figure 1. Again, the agreement between CFD-based prediction and experiment is quite good in terms of coolant surface coverage, while results in terms of the level of cooling effectiveness are overpredicted near the hole. Coverage is matched perfectly in case of rows S3 through S5, see Figures 6(i) and 6(j). In the CFD for rows P4 through P6, see Figures 6(f) through 6(h), the surface patch covered by coolant is slightly shifted away from the pressure side of the airfoil. This tendency is also visible in the corresponding experimental results, but not to the same extent. Apparently, the secondary flow near the endwall, which due to the lateral pressure gradient tends to defer the coolant flow towards the suction side, is overpredicted in the CFD. The deviation is less pronounced for the rows that are located further downstream in the passage.

Looking at the experimental result for rows P6 and S3 the significant level of film cooling effectiveness upstream of the cooling rows again indicates the presence of heat conduction from cavity to flowpath, as has already been discussed in the previous section. This effect is not included in the CFD model and therefore unresolved.

Cavity A - Cooling rows upstream of the passage

The results for coolant rows fed through cavity A are given in Figure 7. Upstream of the profile leading edge towards the pressure side of the airfoil, there is a significant influence of the leading edge horseshoe vortex. This is apparent in both the experimental and the computational results, see Figures 7(a), 7(b), 7(f) and 7(g). However, the CFD overestimates the horseshoe vortex effect which leads to a cooling coverage mismatch between CFD and experiments. The coolant gets closer to the leading edge region in the experiments than in the CFD. This is most apparent for cooling hole rows P1 and P2, see Figures 7(a), 7(f) and 7(b), 7(g) respectively. The same secondary flow overprediction could already be seen in the CFD results for rows P4 through P6, though to a much lesser extent.

The reason for this discrepancy can be seen in Figure 8, which shows a comparison of surface oil-flow visualization on the endwall with wall-streamlines obtained from the CFD. Near the leading edge, the flow actually moves in a direction opposite to the direction of the approach flow. The red line indicates the borderline between approach flow and adverse flow direction based on the oil flow picture. The yellow lines, which indicate wall streamlines obtained from the CFD obviously overpredict this effect.

Cooling rows S1 and S2, from which the coolant is drawn towards the suction side of the airfoil, are hardly influenced by this horseshoe vortex effect. The cooling coverage predicted by the CFD matches the coverage in the experiments very well, see Figures 7(d), 7(i) and 7(e), 7(j) respectively.

However, for all cases, there appears to be a significant disagreement in the level of cooling effectiveness. The CFD predicts much higher cooling effectiveness than was detected in the experiment. This deviation is again attributed to the negligence of the heat exchange between main flow and plenum through the endwall plate. Note that only a slight effect on discharge temperature has a significant effect on cooling effectiveness, given that the total temperature difference is only on the order of 20K. Whether or not the uncertainty in coolant discharge temperature is the only reason for the overprediction of film cooling effectiveness observed in this study can only be determined based on additional experimental validation cases. To reduce the influence of discharge temperature uncertainty on cooling effectiveness results, experimental investigations with higher temperature differences between coolant and main flow should be considered. This will be focus of future work.

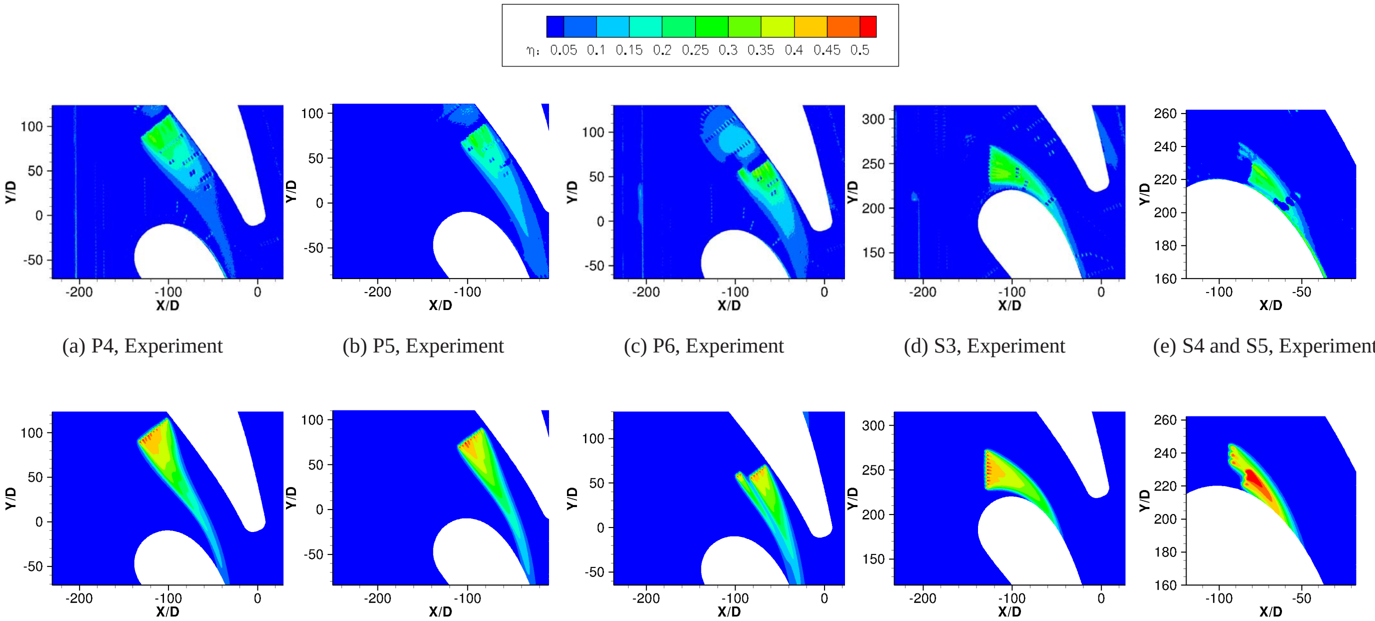

(a) P4, Experiment (b) P5, Experiment (c) P6, Experiment (d) S3, Experiment (e) S4 and S5, Experiment

(f) P4, CFD (g) P5, CFD (h) P6, CFD (i) S3, CFD (j) S4 and S5, CFD

FIGURE 6. Cavity B and E cooling hole rows P4-P6, S3-S5

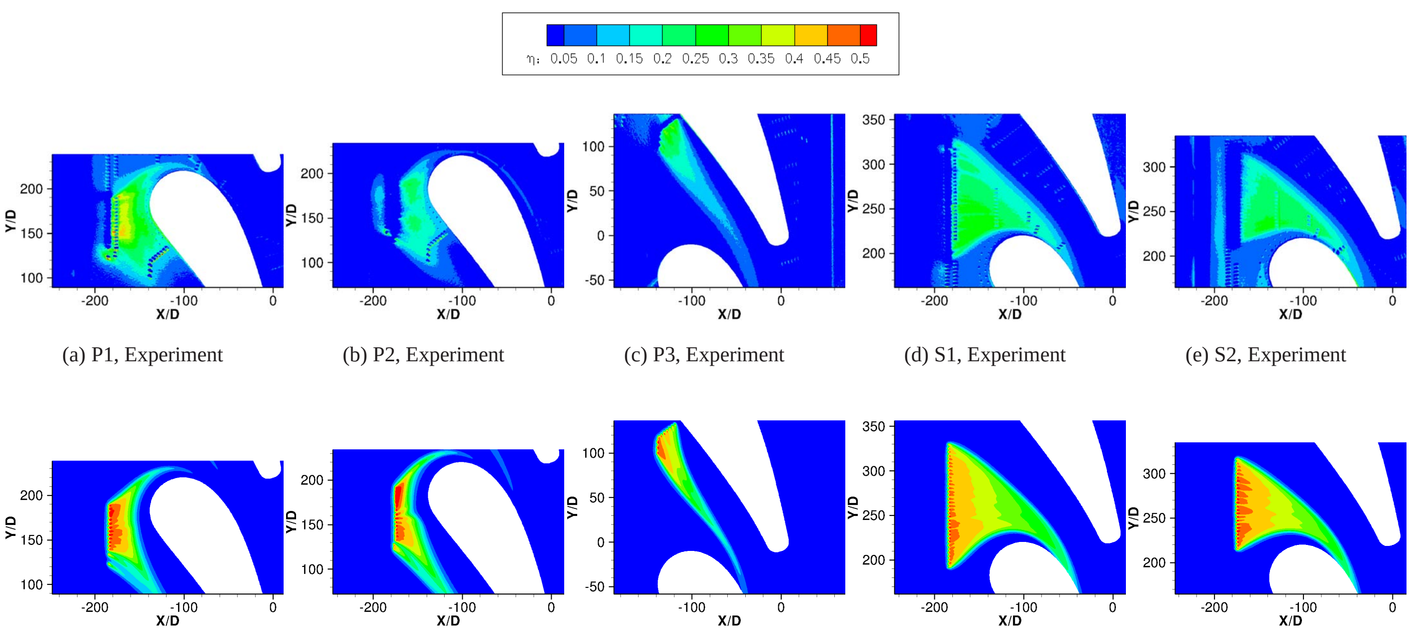

(a) P1, Experiment (b) P2, Experiment (c) P3, Experiment (d) S1, Experiment (e) S2, Experiment

(f) P1, CFD (g) P2, CFD (h) P3, CFD (i) S1, CFD (j) S2, CFD

FIGURE 7. Cavity A cooling hole rows P1-P3, S1 and S2

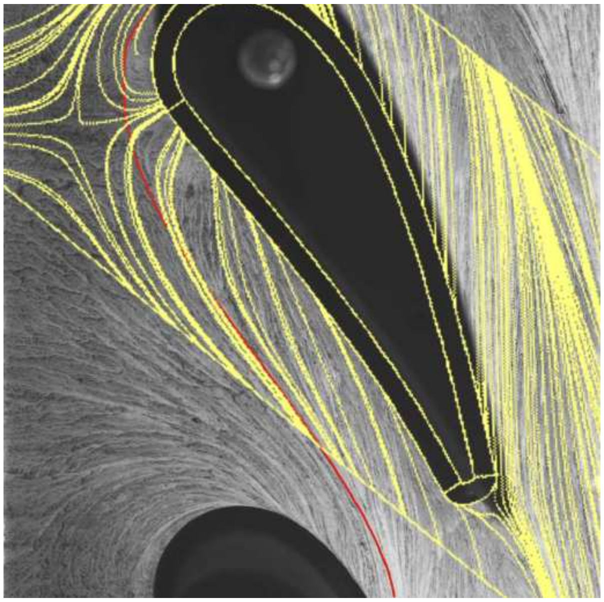

FIGURE 8. Surface oil flow picture (single red line indicates one streamline) vs. CFD wall streamlines (multiple yellow lines)

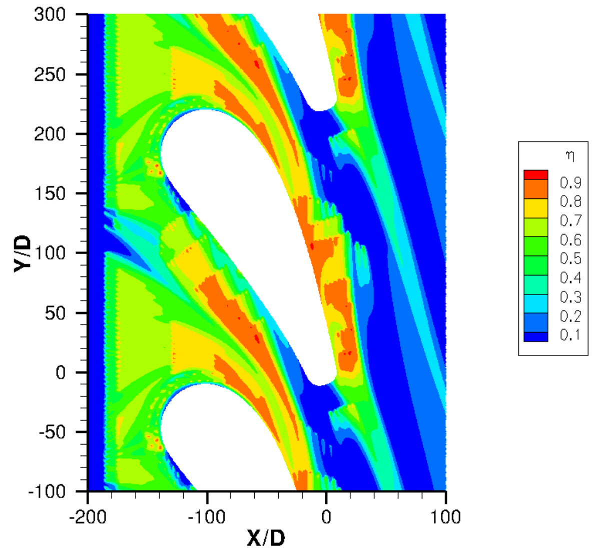

FIGURE 9. Full coverage film cooling simulation using film cooling model

Full coverage film cooling simulation

To show the capability of the film cooling model to run full coverage film cooling simulations, a CFD calculation was performed in which all 253 endwall cooling holes were activated. The result of this study is shown in Figure 9.

This calculation, as well as all previous calculations was performed using the identical computational mesh, i.e. remeshing the computational domain is not necessary when running different types of film cooling configurations. The overhead caused by the film cooling model is further rather independent of the number of film cooling holes modeled. The distributed source terms, which are used to introduce the coolant flow into the computational domain, are calculated only once, prior to the actual solver run and then modified as part of the local integral balance correction during the first 3 iterations. These operations scale linearly with the number of cooling holes.

On average, activating the film cooling model increased computational time by 8% to 12%. There is no indication that the number of cooling holes significantly influences this overhead. Calculations were executed on 2 Quad-Core CPUs (AMD Opteron Processor 2384) and took approximately 10 hours to converge, provided that the converged solution without film cooling was used as initial guess. The average overhead of about 10% has been calculated based on the time it took to complete 200 iterations, which was usually sufficient for convergence. The overhead strongly depends on the number of iterations. The more iterations are considered, the smaller the overhead, as the film cooling model only slows down the calculation during the first iterations.

CONCLUSION

The CFD-based film cooling model by auf dem Kampe and Völker [11] using distributed volumetric source terms with local integral flux conservation has successfully been applied to a gas turbine relevant test case. A linear vane cascade with endwall film cooling served as a validation basis. Various rows of cooling holes were investigated separately.

In most cases, the comparison between CFD and experiment was well in terms of coolant coverage. If coolant coverage was not predicted correctly, it could clearly be attributed to an overprediction of near wall secondary flows by the CFD. It is therefore not a flaw of the film cooling model.

The level of predicted cooling effectiveness tended to be slightly overpredicted by the film cooling model. These deviations have mainly been attributed to the uncertainty in coolant discharge temperature, which significantly impacts film cooling effectiveness. This is particularly true for experimental setups with small temperature differences between main flow and coolant. The fact that significant heat transfer from main flow path to plenum takes place by means of heat conduction through the endwall material could be seen in several of the experimental results. This influence has not been accounted for in the calculation of coolant discharge temperatures which helps explain the cooling effectiveness overprediction. Additionally, this conduction effect leads to slightly elevated cooling effectiveness on the endwall above the coolant cavities. Since heat conduction from main flow path to cavity has not been included in CFD model, this effect could not be resolved. Future work will be directed at additional validation cases. These additional cases should feature a higher temperature difference between coolant and mainflow and should be less influenced by heat conduction between plenum and main flow.

It has been shown that the film cooling model is capable of simulating complex and gas turbine relevant flow situations under the influence of film cooling at manageable computational cost. Different film cooling configurations can be investigated easily with very little modeling effort using the same computational mesh.

Further validation and development of the film cooling model will be focus of future work in order to make it a reliable tool for surface temperature predictions during the thermal design of film cooled components. Results presented in this paper indicate that the approach itself is an important step in the right direction and that further work will help leverage the full potential of the film cooling model by auf dem Kampe and Völker [11].

ACKNOWLEDGMENT

The authors would like to thank Prof. Dr. Michael Crawford and Dr. Andreas Heselhaus for sharing their heat transfer expertise. Prof. Dr. Konrad Vogeler's (TU Dresden) support of this work is gratefully acknowledged.

PERMISSION FOR USE

REFERENCES

[1] L'Ecuyer, M., and Soechting, F., 1985. "A Model for Correlating Flat Plate Film Cooling Effectiveness Data for Rows of Round Holes". Heat Transfer and Cooling in Gas Turbines, AGARD-CP-390, Paper 19.

[2] Baldauf, S., 2001. "Filmkühlung thermisch höchstbelasteter Oberflächen: Korrelation thermographischer Messungen". PhD thesis, Universität Karlsruhe.

[3] Colban, W., and Thole, K., 2007. "Influence of Hole Shape on the Performance of a Turbine Vane Endwall Film-Cooling Scheme". *Int. J. Heat Fluid Fl.*, ***28***, pp. 341–356.

[4] Colban, W., Thole, K., and Händler, M., 2007. "Experimental and Computational Comparisons of Fan-Shaped Film Cooling on a Turbine Vane Surface". *J. Turbomach.*, ***129***, pp. 23–31.

[5] Goormans-Francke, C., Carabin, G., and Hirsch, C., 2008. "Mesh Generation for Conjugate Heat Transfer Analysis of a Cooled High Pressure Turbine Stage". ASME Paper No. GT2008-50660.

[6] Miller, K. L., and Crawford, M. E., 1984. "Numerical Simulation of Single, Double, and Multiple Row Film Cooling Effectiveness and Heat Transfer". ASME Paper No. 84-GT-112.

[7] Heidmann, J. D., and Hunter, S. D., 2001. Coarse Grid Modeling of Turbine Film Cooling Flows Using Volumetric Source Terms. Tech. Rep. NASA/TM-2001-210817.

[8] Dahlander, P., 2001. "Source Term Model Approaches to Film Cooling Simulations". PhD thesis, Chalmers University of Technology.

[9] Burdet, A., Abhari, R. S., and Rose, M. G., 2005. "Modeling of Film Cooling - Part II: Model for Use in 3D CFD". ASME Paper No. GT2005-68780.

[10] Tartinville, B., and Hirsch, C., 2008. "Modelling of Film Cooling for Turbine Blade Design". ASME Paper No. GT2008-50316.

[11] auf dem Kampe, T. G., and Völker, S., 2010. "A Model for Cylindrical Hole Film Cooling: Part II - Model Formulation, Implementation and Results". ASME Paper No. GT2010-22788.

[12] auf dem Kampe, T. G., Zehe, F. N., and Völker, S., 2010. "A Model for Cylindrical Hole Film Cooling: Part I - A Correlation for Jet-Flow with Application to Film Cooling". ASME Paper No. GT2010-22787.

[13] auf dem Kampe, T. G., Völker, S., Sämel, T., Heneka, C., Ladisch, H., Schulz, A., and Bauer, H.-J., 2011. "Experimental and Numerical Investigation of Flow Field and Downstream Surface Temperatures of Cylindrical and Diffuser Shaped Film Cooling Holes". ASME Paper No. GT2011-45106.

[14] Heneka, C., Schulz, A., Bauer, H.-J., Heselhaus, A., and Crawford, M. E., 2010. "Film Cooling Performance of Sharp-Edged Diffuser Holes with Lateral Inclination". ASME Paper No. GT2010-23090.

[15] Kunze, M., Vogeler, K., Brown, G., Prakash, C., and Landis, K., 2009. "Aerodynamic and Endwall Film Cooling Investigations on a Highly Loaded Gas Turbine Vane Applying Temperature-Sensitive Paint". ASME Paper No. GT2009-59412.

[16] Kunze, M., Preibisch, S., Vogeler, K., Landis, K., and Heselhaus, A., 2008. "A New Test Rig for Film Cooling Experiments on Turbine Endwalls". ASME Paper No. GT2008-51096.

[17] Menter, F., 1994. "Two-Equation Eddy-Viscosity Turbulence Models for Engineering Applications". *AIAA J.*, ***32***, pp. 1598–1605.